ChemComm

Cite this: *Chem. Commun.*, 2011, **47**, 10874–10885

www.rsc.org/chemcomm

HIGHLIGHT

Recent progress in actinide borate chemistry

Shuao Wang,[a] Evgeny V. Alekseev,[b] Wulf Depmeier[c] and Thomas E. Albrecht-Schmitt*[a]

DOI: 10.1039/c1cc14023j

The use of molten boric acid as a reactive flux for synthesizing actinide borates has been developed in the past two years providing access to a remarkable array of exotic materials with both unusual structures and unprecedented properties. $[ThB_5O_6(OH)_6][BO(OH)_2]\cdot 2.5H_2O$ possesses a cationic supertetrahedral structure and displays remarkable anion exchange properties with high selectivity for TcO_4^-. Uranyl borates form noncentrosymmetric structures with extraordinarily rich topological relationships. Neptunium borates are often mixed-valent and yield rare examples of compounds with one metal in three different oxidation states. Plutonium borates display new coordination chemistry for trivalent actinides. Finally, americium borates show a dramatic departure from plutonium borates, and there are scant examples of families of actinides compounds that extend past plutonium to examine the bonding of later actinides. There are several grand challenges that this work addresses. The foremost of these challenges is the development of structure-property relationships in transuranium materials. A deep understanding of the materials chemistry of actinides will likely lead to the development of advanced waste forms for radionuclides present in nuclear waste that prevent their transport in the environment. This work may have also uncovered the solubility-limiting phases of actinides in some repositories, and allows for measurements on the stability of these materials.

[a] *Department of Civil Engineering and Geological Sciences and Department of Chemistry and Biochemistry, University of Notre Dame, 156 Fitzpatrick Hall, Notre Dame, Indiana 46556, USA. E-mail: talbrec1@nd.edu*
[b] *Forschungszentrum Jülich GmbH, Institute for Energy and Climate Research (IEK-6), 52428 Jülich, Germany. E-mail: e.alekseev@fz-juelich.de*
[c] *Institut für Geowissenschaften, Universität zu Kiel, 24118 Kiel, Germany*

Shuao Wang

Shuao Wang received his BSc in Material Chemistry from the Department of Materials Science and Engineering in University of Science and Technology of China in 2007. He worked in Prof. Beifang Yang's lab as an undergraduate researcher focusing on wide band gap semiconductor nano-materials from 2005 to 2007. He then joined Prof. Thomas E. Albrecht-Schmitt's research group as a PhD student at the University of Notre Dame focusing on the solid state chemistry of actinide oxo-anion compounds. His research project right now is "new insights in actinide borate chemistry."

Evgeny V. Alekseev

Evgeny V. Alekseev was born in Murom, USSR, in 1980. He received a Diploma with Honors in Chemistry (2002) and PhD (2004) from the State University of Nizhny Novgorod (Russia). He moved to the University of Kiel (Germany) to work in group of Prof. Wulf Depmeier in 2005. In 2009 he was a visiting scientist at the group of Prof. Thomas E. Albrecht-Schmitt, University of Notre Dame, USA. Since March 2011 he has been a research scientist at the Institute of Energy and Climate Research–Nuclear Safety Research and Reactor Technologies (IEK-6), Forschungszentrum Jülich (Germany).

1. Introduction

The terrestrial abundance of boron, mostly existing as borates, is 10 ppm.[1] Large borate deposits occur as the result of the evaporation of ancient oceans and seas. Uranium, the heaviest naturally occurring element, has a relatively low terrestrial abundance at 2.7 ppm.[2] However, a variety of processes concentrate uranium in the Earth's crust, and numerous uranium minerals with most of the common oxo-anions have been discovered.[3–5] Surprisingly, borate and uranium deposits have never been found to co-exist, and there are no known uranium borate minerals. However, the disposal of nuclear waste results in large amounts of actinides from uranium to curium and borates being artificially concentrated together for the first time.

Except for Russia, which has produced aluminophosphate glasses for decades, borosilicate glasses have become the only waste form for high-level radioactive waste.[6,7] In the United States, the vitrification of nuclear waste using borosilicate glasses started in 1996 primarily at the Savannah River Site, and this process is estimated to continue for at least two decades to vitrify the waste associate with the production of plutonium for nuclear weapons.[8] It has been recognized that both processing techniques and high actinide content in the glasses can lead to the formation of crystalline products such as silicates and borates within these glasses, which may lower the chemical durability and the integrity of the glass.[7,8]

One of the well-known salt deposits is the Salado formation near Carlsbad, New Mexico where the concentration of borate, predominately in the form of H_3BO_3, $B(OH)_4^-$, and $B_4O_7^{2-}$ reaches concentrations as high as 166 ppm in intergranular brines.[9] Located within this deposit is the United States' only repository for nuclear defense waste known as the Waste Isolation Pilot Plant (WIPP). WIPP presents a unique environment whereby large quantities of not only uranium, but also lesser amounts of the transuranium elements neptunium, plutonium, americium, and curium, will eventually be able to react with the brines, potentially leading to the formation of actinide borate compounds. Recent complexation and speciation studies of neodymium(III), which acts as a surrogate of An(III) (An = actinide) in simulated WIPP brines have shown that borate competes with carbonate for An(III) complexation under the repository conditions.[10] The presence of the decaying nuclear waste will lead to heating beyond the ambient conditions in the deposit, and therefore the reactions of actinides with borates at moderate temperatures are important reactions to study in order to predict the fate of actinides in the repository.

Finally, the recent earthquake and tsunami in Japan that crippled the *Fukushima Daiichi* nuclear power plant caused the release and dispersion of radioactive materials. In an effort to prevent the nuclear fuel rods from melting down, large amounts of sea water and boric acid were pumped into the reactors. It appears that the cladding of the fuel rods failed, exposing the hot fuel to concentrated boric acid. As a result, actinides potentially reacted with borates to yield actinide borates.

Despite the importance of understanding all these mechanisms for forming actinide borates, there are very few examples of well-characterized actinide borates. In fact, until very recently there were no examples of transuranium borates. The first crystalline actinide borate compound reported was $K_6[UO_2\{B_{16}O_{24}(OH)_8\}]\cdot 12H_2O$, which was crystallized *via* the room temperature evaporation of water.[11] This compound adopts a complicated molecular structure consisting of a uranyl core surrounded by a 16-borate ring.[11] From 1986 to 1991, Gasperin synthesized seven actinide borate compounds, including $UO_2(B_2O_4)$, $Li(UO_2)BO_3$, $Na(UO_2)BO_3$, $Ca(UO_2)_2(BO_3)_2$, $Mg(UO_2)B_2O_5$, $Ni_7(UO_2)(B_4O_{14})$, and ThB_2O_5 by using molten B_2O_3 as a flux in high temperature (>1000 °C) reactions.[12–18] These actinide borates contain BO_3 triangles, except for $Ni_7(UO_2)(B_4O_{14})$, which contains both BO_3 triangles and BO_4 tetrahedra.[16] No new actinide borates were reported for almost 20 years. More importantly, no actinide borates were synthesized at slightly elevated temperatures. One of the reasons is that the crystallization of actinide borate compounds can be greatly affected by the hydrolysis of actinides in solution.[19]

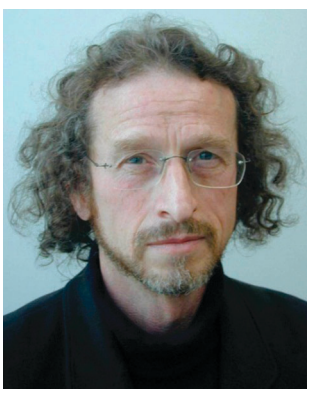

Wulf Depmeier

Wulf Depmeier was born in Sulingen, Germany, in 1944. He earned a PhD in mineralogy-crystallography from the University of Hamburg in 1973. After post-doctoral research at the Universities of Konstanz (Germany), Geneva (Switzerland) and Karlsruhe (Germany) (1974–1984), he became Professor of Crystallography at the Technical University Berlin (1985–1991) and the University of Kiel (1992–2010). He is currently chairman of the IUCr Commission on Inorganic and Mineral Structures. He is mainly interested in phase transitions, including modulated structures in layered and microporous materials, as well as in the structures of complex natural silicates and actinyl compounds.

Thomas E. Albrecht-Schmitt

Thomas E. Albrecht-Schmitt received his BS in chemistry from Southwest Minnesota State University in 1993. He earned his PhD in inorganic chemistry at Northwestern University under the direction of James A. Ibers in 1997. After a short post-doc at the University of Illinois with John R. Shapley, he began his independent career at Auburn University where he rose through the ranks to full professor. In 2009 he moved to the University of Notre Dame as the Frank M. Freimann chair. His research interests include all aspects of lanthanide and actinide chemistry, materials chemistry, environmental chemistry, and crystallography.

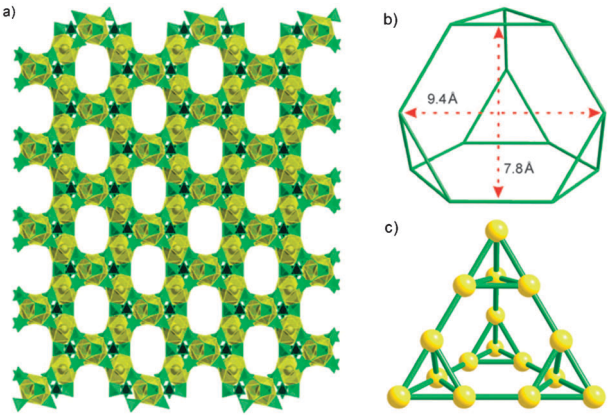

Fig. 1 (a) A view along [110] of the 3D structure of **NDTB-1**. The disordered $H_2BO_3^-$ anions and water residing in the channels have been omitted for clarity. (b) Cage topology of the structure of **NDTB-1**. (c) Topology of the supertetrahedral 3D framework based on Th atoms (yellow).

In order to overcome this synthetic challenge, we adopted boric acid as a low temperature flux where it serves as both a reagent and the reaction medium. By using this synthetic technique, we have already successfully synthesized a thorium(IV) borate, $[ThB_5O_6(OH)_6][BO(OH)_2]\cdot 2.5H_2O$ (**NDTB-1**), with a cationic framework structure and remarkable anion exchange capabilities,[20,21] a large family of uranyl(VI) borates,[22–26,31] several neptunium borates with a variety of combinations of single valence states or mixed/intermediate valence states,[26–29,31] several plutonium borates with plutonyl(VI) or plutonium(III) metal centers,[26,29,30,32] and a single example of an americium(III) borate.[32] In this article, we will provide an overview of the synthetic puzzles, topological classifications, structure-property relationships, and potential applications of all of the actinide borate compounds that have been recently reported by us. There is not sufficient space to highlight all of these compounds, so compounds that illustrate the unique characteristics of this system will be discussed.

2. Thorium borate

Thorium borates are poorly described in the literature. Except for some rare examples of thorium-rich minerals,[33–37] there is only one crystallographically characterized example known, ThB_2O_5, which was prepared *via* the high temperature B_2O_3 flux method.[18] This paucity is surprising in light of the fact that a thorium borate was reported by Berzelius in 1826. This compound was thought to be $Th_3(BO_3)_4$, but the evidence for this is not convincing.[38] We made use of the molten boric acid flux to synthesize the **NDTB-1** (Notre Dame Thorium Borate-1), with the formula, $Th[B_5O_6(OH)_6](H_2BO_3)\cdot 2.5H_2O$.[20]

One of the most important aspects of this compound is that its 3D-framework possesses a positive charge with extra framework $H_2BO_3^-$ anions residing within channels of the framework to balance the charge. This is interesting, since materials with extended structures are typically based on anionic networks where the charge is balanced by cations that fill the space between the anionic portions of the structure. The best known exceptions to this concept are the layered double hydroxides (LDH's).[39–41] Owing to their unique structural character in that there are metal hydroxide slabs with interlayer anions that can be easily exchanged, the LDH family are extremely important for a variety of environmental applications such as the removal of key environmental anionic contaminants from solution. Framework collapse is typically observed during anion exchange. However, this is overcome in the recently discovered materials **NDTB-1** and $YbO(OH)_6Cl\cdot 2H_2O$,[42] and several cationic metal organic frameworks containing Ag(I) or Cu(I).[43]

2.1 Structural features of NDTB-1

The structure of **NDTB-1** is a porous supertetrahedral 3D framework crystallized in the $Fd\bar{3}$ space group. The building blocks of this framework are twelve-coordinate Th^{4+} ions surrounded by BO_3 and BO_4 units. The BO_4 tetrahedra chelate the thorium centres, while the BO_3 groups occupy single vertices (Fig. 1a). All borate oxygen atoms are bound to thorium. The thorium atoms reside on $\bar{3}$ sites, thus yielding a nearly regular icosahedral coordination geometry. The borate anions are polymerized, and form $B_{10}O_{24}$ clusters with three-fold symmetry that bridge between the thorium centers. The bridging of the thorium centers by the borate clusters creates a supertetrahedral framework (Fig. 1c).

Thorium atoms and crown-like $B_{10}O_{24}$ groups do not fill all of the space in the supertetrahedra, and as a result of this architecture, large free voids in the structure of **NDTB-1** are observed. The result of such a combination is a regular 3D framework with a system of channels and cages. The channels of **NDTB-1** extend along cubic [110] directions as shown in Fig. 1a. These channels intersect in the center of the supertetrahedra to form cages. The gates into the intersecting chambers have a hexagonal form and are 9.4 × 7.8 Å in size (Fig. 1b). Each cage has four identical gates and forms a truncated tetrahedron. The free void volume in **NDTB-1** is 43%, which makes it the second most porous actinide compound known to date.[44–46]

Both single crystal X-ray diffraction and charge-balance considerations show that this supertetrahedral framework possesses a positive charge with some highly disordered protonated BO_3 groups residing in the channels and cages to balance the charge, which is also confirmed by ^{11}B MAS NMR spectroscopy.[20] Within the cationic framework, the channels form a network that pierces the whole structure and allows facile anionic transport for the exchange processes while the cages can trap these anions with suitable charge and size.

2.2 Anion exchange studies of NDTB-1

Anion exchange experiments were conducted with a variety of common anions including halides (Cl^-, Br^-, I^-), and oxo-anions such as MnO_4^-, TcO_4^-, ReO_4^-, CrO_4^{2-}, $Cr_2O_7^{2-}$, SeO_4^{2-}, SeO_3^{2-}, IO_3^-. These studies, which combined inductively coupled plasma mass spectrometry (ICP-MS), energy-dispersive

X-ray spectroscopy (EDS), and single-crystal and powder X-ray diffraction, revealed not only that anion exchange takes place, but that the structure remains intact throughout the exchange. More impressive is the fact that single crystals retain their integrity throughout the exchange, although with these small anions, disorder in the channels remains a crystallographic problem. Exchange experiments conducted with a variety of highly colored anions, such as MnO_4^-, CrO_4^{2-}, and $Cr_2O_7^{2-}$, resulted in the single crystals showing the color of the transition metal anions within a few minutes (Fig. 2). The crystals can be cut, and the interior shows the same color as the surface.[20]

The critical anion exchange experiments involve replacement of the extra-framework borate anions with TcO_4^-. The uptake of the TcO_4^- by **NDTB-1** was monitored using the charge-transfer bands (290 nm) in the UV region of the spectrum. These studies of as-synthesized intact crystals of **NDTB-1** show rapid uptake of TcO_4^- from solution. (Fig. 3).[20]

More importantly, **NDTB-1** was tested on simulated Hanford Site nuclear waste solutions, which contained carbonate, sulfate, chloride, nitrate, and nitrite anions in addition to the TcO_4^- anion.

Despite the presence of more than 300-fold excesses of chloride and nitrate ions, and a 15-fold excess of nitrite ions in a simulated low-activity melter recycle stream, **NDTB-1** selectively removed pertechnetate TcO_4^- anions with a distribution coefficient K_d of 16.2–22.9 mL g^{-1} (for TcO_4^- anions) from the solution.[21] This exchange selectivity for TcO_4^- anions is unprecedented, and can be understood by the ability of **NDTB-1** to trap TcO_4^- anions within the cavities in the cationic framework as demonstrated by ^{99}Tc NMR (*vide infra*).

2.3 ^{99}Tc-MAS-NMR spectroscopy of TcO_4^- exchanged NDTB-1

The first ^{99}Tc MAS NMR spectra of TcO_4^- exchanged **NDTB-1** was recently reported to probe the behavior of the TcO_4^- anions within the cationic framework.[21] The spectra show the presence of at least two sites where TcO_4^- anions reside in the material (Fig. 4). There are two signals in the spectra. One is a narrow peak near 0 ppm, with approximately 1.5 kHz full-width at half-maximum (FWHM) at 293 K which can be assigned to the TcO_4^- anions residing in the channels of **NDTB-1**. The other one is a broader peak centered near −40 ppm, with approximately 4.6 kHz FWHM at 293 K which can be assigned to TcO_4^- anions being trapped in the cages of **NDTB-1**. The intensity of the narrow peak diminishes markedly with decreasing temperature, consistent with its assignment to TcO_4^- anions that undergo rapid, near-isotropic tumbling near room temperature. The broader signal is accompanied by sets of spinning sidebands at all temperatures, and accounts for most of the signals in the spectra. This suggests most of the TcO_4^- anions exchanged from the solution are trapped in the cages of **NDTB-1**.

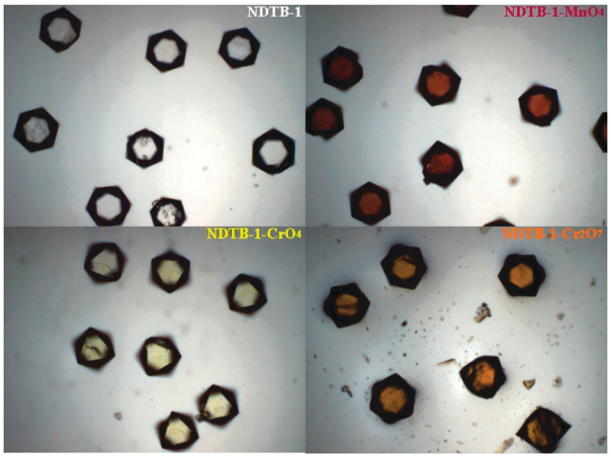

Fig. 2 Photos of crystals of NDTB-1, MnO_4^- exchanged NDTB-1, CrO_4^{2-} exchanged NDTB-1, $Cr_2O_7^{2-}$ exchanged NDTB-1.

3. Uranium borate

Uranyl borates represent a fascinating group of zero-, two-, and three-dimensional materials.[11–17,22–26] A variety of synthetic methods have been employed to prepare these compounds, and the conditions under which these solids form leads to their subdivision into three categories. The first group is a series of chiefly centrosymmetric borates that are primarily constructed from UO_6 tetragonal bipyramids and/or UO_7 pentagonal bipyramids and BO_3 triangles.[12–17] These compounds are derived from high-temperature B_2O_3 melts. The second category has only one single representative, $K_6[UO_2\{B_{16}O_{24}(OH)_8\}]\cdot 12H_2O$, and this compound consists of isolated clusters composed of a cyclic polyborate surrounding an uranyl core. It forms by slow evaporation of aqueous solutions containing UO_2^{2+} and borate at room temperature.[11] The third group has been prepared by us using boric acid fluxes at relatively low temperatures (*ca.* 180–280 °C).[22–26] Herein, we will only discuss the synthesis, structural topologies, and physical properties of the uranyl(VI) borates of the third group.

3.1 New uranyl borates

Molten boric acid flux reactions have proven to be a safe and facile way to prepare actinide borate compounds. Particularly, the boric acid flux reactions of uranyl nitrate with alkali metal or pseudo alkali metal (Ag^+ and Tl^+) nitrates have already generated more than 37 novel uranyl borate compounds by simply changing the reaction conditions including the reaction temperature, reaction time, and stoichiometry of starting materials.[22–26] Further incorporation of the F^- anion in the starting materials can lead to a novel uranyl fluoroborate family.[31] Moreover, by adopting methyl boronic acid as an alternative flux which has a lower melting point, the first actinide boronate with the formula of $UO_2(CH_3BO_2)(H_2O)$ has been prepared.[28]

3.2 Topological classifications of the structures of the novel uranyl borates family

All uranyl borates we obtained to date are based on uranyl polyborate sheets. These sheets are formed by the corner condensation of BO_4 tetrahedra and BO_3 triangles. An example of such an arrangement for a typical uranyl borates is shown in Fig. 5. This is a polyborate

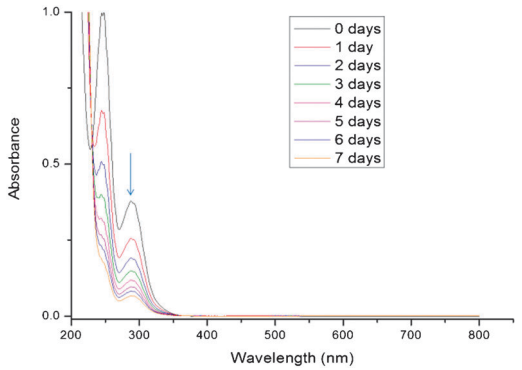

Fig. 3 UV-vis spectra of TcO_4^- solution exchanged with **NDTB-1**.

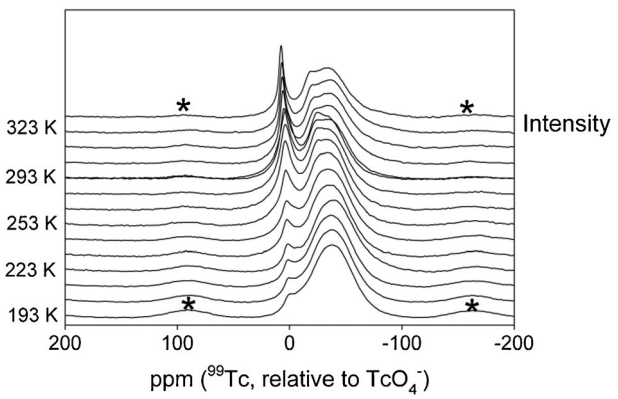

Fig. 4 Variable-temperature (VT), solid-state MAS ^{99}Tc NMR spectra of **NDTB-1** that had been ion-exchanged with TcO_4^- solution to replace the extra-framework $H_2BO_3^-$ anions.

sheet observed in the structure of $Rb_2[(UO_2)_2B_{13}O_{20}(OH)_5]$,[24] and presented in skeletal and polyhedral modes in Fig. 5a and b, respectively. The uranyl cations reside in the triangular holes within the polyborate sheets. It is possible to classify the type of these sheets based on the super triangle-like groups linked *via* BO_3 triangles selected within dashed red circle. The super-triangles are based on three BO_4 tetrahedra in the structure of $Rb_2[(UO_2)_2B_{13}O_{20}(OH)_5]$ and in several other compounds. However, one of the borate units within the super-triangle can be substituted by BO_3 triangles in other uranyl borate phases. The borate units which link the super-triangles are not necessarily BO_3 and can also be substituted by BO_4 tetrahedra. Thus, the ratio between BO_3 and BO_4 units within the polyborate sheets is a key of the structural diversity that allows many possible types of polyborate sheets with similar topologies in actinide borate phases.

The coordination environment around the uranyl cation within the sheets can also be used to classify the sheet type. Typically, each uranyl cation is surrounded by nine neighbouring borate units (Fig. 5b). Different types of sheets can be achieved by different numbers of BO_3 triangles and BO_4 tetrahedra and their coordination arrangements around the uranyl cations. For example, in the uranyl polyborate sheets of $Rb_2[(UO_2)_2B_{13}O_{20}(OH)_5]$, there are six BO_4 tetrahedra and three BO_3 triangles around each uranyl cation. Based on these aspects, up to date we have observed 11 different sheet types for all actinide borate compounds (Fig. 6, types A–M) that are further complicated by the fact that many are enantiomorphic.

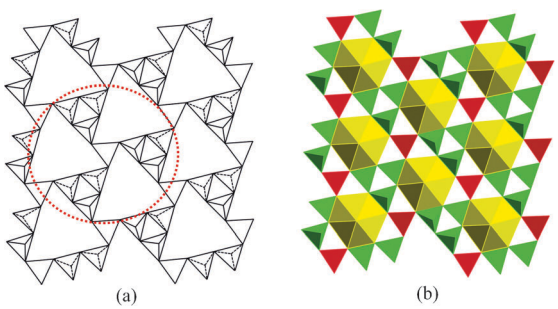

Fig. 5 Skeletal (a) and polyhedral (b) representations of the polyborate sheet.

For a typical uranyl borate, there are additional borate units that extend perpendicularly to the planes of uranyl borate polyborate sheets to form a layered structure, or these borate units bridge between sheets to form a three-dimensional framework structure. A structural hierarchy based on the sheet extending and bridging is also observed in actinide borates. For example, in the Tl-uranyl borate system, the extending BO_3 triangles are tuning the structures by forming single layers, doubled layers, and 3D frameworks. This feature makes actinide borates unique among all known actinide systems.

The structural features and interrelationships of this large group of materials can be represented by lithium and silver uranyl borates. Both lithium and silver uranyl borate families are represented only by single phases–$Li[UO_2B_5O_9]\cdot H_2O$ and $Ag[(UO_2)B_5O_8(OH)_2]$.[25] They are closely related in chemical composition and in structural aspects despite the large difference in ionic radii between Li^+ and Ag^+. The crystal structure fragments of Li and Ag uranyl borates are shown in Fig. 7a and b, respectively. Both phases are based on the same G-type of polyborate sheets (Fig. 6). There are additional BO_3 triangles extending perpendicular to the uranyl borate sheets in these structures. However, they play different roles in Li and Ag uranyl borates. In the structure of the lithium phase, BO_3 triangles link uranyl borate sheets into a 3D framework, but in the structure of the silver phase they do not. The positions of lithium and silver cations are similar, and they reside between the sheets. There is enough space for water molecules to be present in the structure of $Li[UO_2B_5O_9]\cdot H_2O$ because of the small size of Li

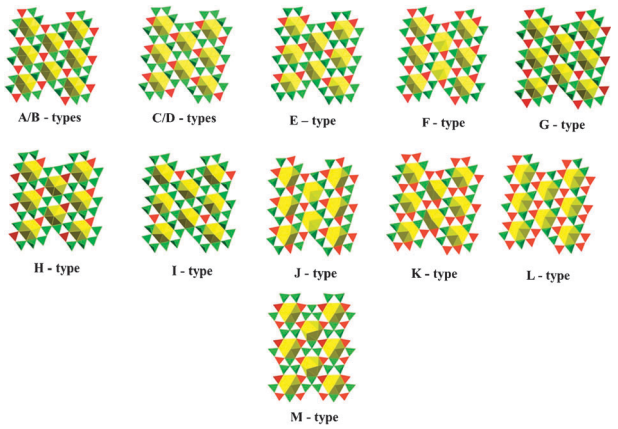

Fig. 6 Polyhedral representations of all polyborate sheet types found to date in the actinide borate system.

cations; while in silver phase water molecules are absent. The relationship between described structure types is schematically presented in Fig. 7c. The skeletal representations of polyborate nets in the Ag and Li structure types have been plotted in this Fig. 7c. In order to transform the structures from the Ag-type to Li-type, we need to turn each second layer by 180° in the plane of the sheets (shown by red dashed arrow), and shift these sheets by translations of 1/2 in x and 1/3 in z. As a result of these manipulations the BO_2OH triangles (shown in red) will occupy positions that are very close to the BO_3OH tetrahedra (shown in red).

4. Neptunium borates

As the first transuranium element, neptunium is extremely important because its main isotope ^{237}Np has a long half-life ($t_{1/2} = 2.14 \times 10^6$ years), and in the long-term will be the primary contributor to the calculated dose from spent nuclear fuel stored in repositories.[47] Neptunium can exist in the natural environment in oxidation states of IV, V, and VI; although neptunium under strongly oxidizing or reducing conditions can really range from III to VII.[48] Np(V) is the most stable oxidation state in solution under most common conditions.[48] However, it is known that Np(V) will disproportionate to Np(VI) and Np(IV) under a variety of conditions.[48] The relative stabilities between these oxidation states can be significantly affected by numerous factors such as concentration,[49] temperature,[50] counter ions,[51] radiolysis,[52] and hydrolysis.[19] A significant numbers of known neptunium compounds are mixed-valent containing Np(IV)/Np(V) or Np(V)/Np(VI).[53–57]

Borate is favorably endowed with the ability to coordinate with neptunium metal centers in all possible oxidation states for several reasons. First, the building units of borates, BO_3 triangles and BO_4 tetrahedra tend to polymerize under a variety of conditions to form countless types of polyborate anions which provides numerous bonding modes to possibly coordinate the metal centers with a variety of geometric requirements.[58–62] Second, borate itself is a non-redox-active ligand under most conditions. This provides us an opportunity of controlling or at least predicting the oxidation states of actinides in products by controlling the oxidation states of actinides and the reduction potentials in the starting materials. Herein we will discuss how we synthesized neptunium borates with mixed/intermediate or single valence states.

4.1 Mixed/intermediate-valent neptunium borates

When Np(VI) nitrate reacts with molten boric acid with K^+ or Ba^{2+} at 220 °C, two highly usual mixed/intermediate neptunium borate compounds, $K_4[(NpO_2)_{6.73}B_{20}O_{36}(OH)_2]$ and $Ba_2[(NpO_2)_{6.59}B_{20}O_{36}(OH)_2]\cdot H_2O$ can be isolated.[26] These two compounds contain Np(IV), Np(V), and Np(VI) simultaneously, which serve as the first examples of actinide compounds containing three oxidation states for an actinide element, although several rare compounds containing transition metal elements were known to possess three oxidation states for a same element.[63,64] When Np(V) chloride was used as the starting material, where chloride and borate are the only counter ions in the reaction, $(NpO_2)_4[(NpO_2)_{6.73}B_{20}O_{36}(OH)_2]$ forms, which also contains Np(IV), Np(V), and Np(VI). Based on comparative studies using Np(VI) and Np(V) as the source of neptunium in these syntheses, it has been determined that this compound forms by partial disproportionation of the Np(V) to yield Np(VI) and Np(IV). The fact that this compound forms with many different interlayer cations and from different oxidation states of neptunium suggests that it represents an energetic well.

The structures of $K_4[(NpO_2)_{6.73}B_{20}O_{36}(OH)_2]$ and $Ba_2[(NpO_2)_{6.59}B_{20}O_{36}(OH)_2]\cdot H_2O$ are highly complicated as shown in Fig. 8a. The overall structure is layered with slabs of neptunyl borate separated by K^+ or Ba^{2+} cations. These neptunyl borate layers are based on two sub-layers and approximately 1.6 nm thick which is much thicker than other layered actinide compounds. Within the neptunyl borate layers, there are four distinct neptunium sites. In all cases the neptunium is found in the form of an approximately linear dioxo cation, NpO_2^{n+}. In two of the sites the NpO_2^{n+} cations are coordinated by six oxygen atoms in the equatorial plane to form an NpO_8 hexagonal bipyramid. One NpO_2^{n+} cation is bound by five oxygen atoms to form an NpO_7 pentagonal bipyramid. Bond-valence sum calculations suggest the NpO_8 units being primarily +6 and the NpO_7 units primarily +5. The final NpO_2^{n+} cation is bonded to four oxygen atoms in equatorial plane to yield a tetragonal bipyramid. The core neptunyl unit in this position has Np=O bond distances that average 1.938(14) Å, which are considerably longer than those found in Np(V) compounds, which average 1.83(2) Å. The neptunyl bond distances and the bond-valence sum calculations indicate Np(IV). More importantly, the NpO_6 site is solely held in place by so-called *cation–cation interactions* which describe the scenario that the "yl" oxo atoms from one neptunyl cation bond to a neighbouring neptunium polyhedron in its equatorial plane.[65,66] Not only dioxo Np(IV) unit, but also this CCI-only surrounding coordination environment, were observed for the first time in these compounds. All together, the joining of the NpO_6, NpO_7, NpO_8,

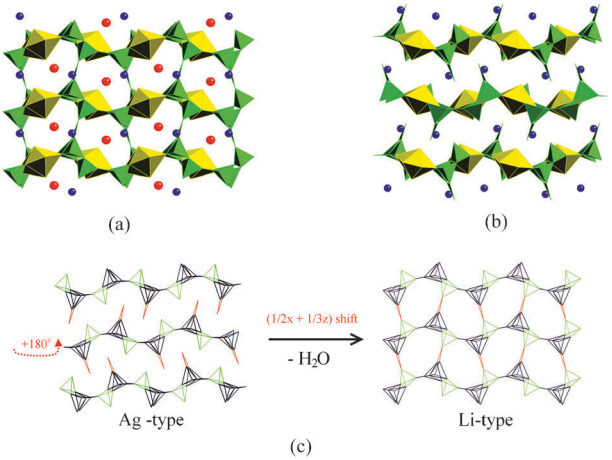

Fig. 7 The crystal structures of $Li[(UO_2)B_5O_9]\cdot H_2O$ (a), $Ag[(UO_2)B_5O_8(OH)_2]$ (b) (UO_8 hexagonal bipyramids are shown in yellow, BO_3 and BO_4 units in green, Li and Ag cations in purple and water molecules in red) and schematic representation of $Li[(UO_2)B_5O_9]\cdot H_2O$ and $Ag[(UO_2)B_5O_8(OH)_2]$ structure type relationships (c).

BO_3, and BO_4 units creates the remarkable neptunyl borate layers.

The UV-vis-NIR spectroscopy measurements taken from crystals of $K_4[(NpO_2)_{6.73}B_{20}O_{36}(OH)_2]$ and $Ba_2[(NpO_2)_{6.59}B_{20}O_{36}(OH)_2]\cdot H_2O$ provided much stronger evidence for the existence of three oxidation states for neptunium in these crystals. Absorption features are present that clearly identify Np(IV), Np(V), and Np(VI) as shown in Fig. 8b. The most important f–f transitions for Np(IV) are the transitions near 700 nm and 800 nm; whereas the Np(V) and Np(VI) transitions are observed near 990 and 1200 nm, respectively.[67] Based on the comparison of the electronic spectroscopy and the crystal structure, the following formula based on formal oxidation states could be proposed, $K_4[(Np^{IV}O_2)_{0.73}(Np^{V}O_2)_2(Np^{VI}O_2)_4B_{20}O_{36}(OH)_2]$ and $Ba_2[(Np^{IV}O_2)_{0.59}(Np^{V}O_2)_2(Np^{VI}O_2)_4B_{20}O_{36}(OH)_2]\cdot H_2O$. Calculations based on the known extinction coefficients and the measured intensities of the primary peaks in the UV-vis-NIR spectrum are consistent with this formulation.

The magnetic susceptibility measurement for the $K_4[(NpO_2)_{6.73}B_{20}O_{36}(OH)_2]$ show the sample to be simply paramagnetic down to the lowest temperature measured. Fitting the susceptibility data assuming Curie–Weiss behavior of non-interacting, localized moments, produces an effective moment of 3.08 ± 0.15 μ_B per Np ion. The theoretical, free-ion effective moments, based on Russell Saunders coupling, are 3.62, 3.58, and 2.54 μ_B for Np(IV), Np(V), and Np(VI), respectively.[68] It is interesting that if the susceptibilities are calculated assuming the free-ion moments weighted by the ratios of crystallographic multiplicities, yields a calculated effective moment of 3.01 μ_B per Np ion, well within the error of the experiment. The presence of neptunyl(V) and/or (IV) is confirmed by these results because these valence states are required to increase the measured value above the 2.54 μ_B theoretical value for Np(VI). This behavior is similar to the mixed-valent Np(IV)/Np(V) selenite, $Np(NpO_2)_2(SeO_3)_3$,[53] and contrasts sharply with most pure Np(V) compounds that either ferromagnetically order <10 K or antiferromagnetically order near 20 K.[69,70]

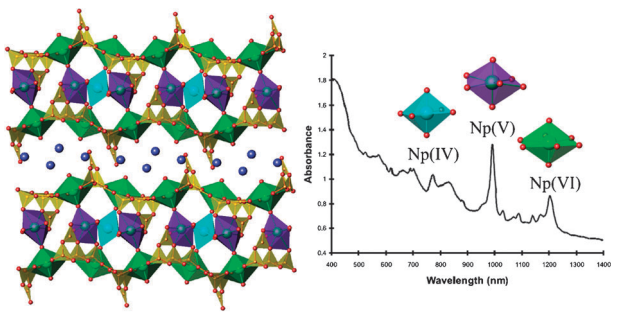

Fig. 8 A depiction of the structure of $K_4[(NpO_2)_{6.73}B_{20}O_{36}(OH)_2]$ or $Ba_2[(NpO_2)_{6.59}B_{20}O_{36}(OH)_2]\cdot 0.6H_2O$ showing $Np^{VI}O_8$ (green), $Np^{V}O_7$ (dark blue), and $Np^{IV}O_6$ (light blue) units linked by BO_3 triangles and BO_4 tetrahedra (a) and UV-vis-NIR spectrum of $K_4(NpO_2)_{6.73}B_{20}O_{36}(OH)_2$ showing regions of f–f transitions that indicate the presence of Np(IV), Np(V), and Np(VI) (b).

4.2 Neptunium(V) borate

The melting point of boric acid is 170.9 °C and this temperature must be exceeded for it to act as a reactive flux. In order to prepare the actinide borates compounds below this temperature, the simplest form of the boronic acid, methyl boronic acid was adopted as an alternative flux which has a much lower melting point within the range of 89–94 °C. In addition, the C–B bond is not thermally robust in general, and boronates are usually readily degraded to borates. Following this synthetic procedure, the first pure Np(V) borate, $NpO_2[B_3O_4(OH)_2]$, has been successfully synthesized which indicates that the temperature is likely to be a key factor for the disproportionation of Np(V) in the borate system.[28]

The crystal structure of $NpO_2[B_3O_4(OH)_2]$ contains sheets of NpO_2^+ pentagonal bipyramids connected through cation–cation interactions. Within the sheets, each NpO_2^+ cation bonds to four other neptunyl cations *via* these interactions to produce the most common CCI bonding mode for all neptunium(V) compounds that contain CCI's.[71] These sheets are further stacked along the *b* axis *via* bridges formed by both BO_3 and BO_4 units to create a three-dimensional framework structure (Fig. 9a). Both Np=O bond distances (1.85(1) Å and 1.81(2) Å) and bond-valence sum (5.14) are consistent with oxidation state assignment of Np(V) in the crystal structure.[71]

The existence of Np(V) in $NpO_2[B_3O_4(OH)_2]$ also can be confirmed by the UV-vis-NIR spectrum (Fig. 9b). As expected, the most important f–f transition for Np(V) at 980 nm is shifted to a longer wavelength at 1013 owing to the

CCI bonds.[66] The key transitions for both Np(IV) and Np(VI) are absent in the spectrum of $NpO_2[B_3O_4(OH)_2]$.[67]

4.3 Neptunium(VI) borate

The counter anions present in the starting materials for making neptunium borates are found to be the key factor for controlling the oxidation states of neptunium in the final products. When nitrate or chloride is present in the boric acid flux reactions, mixed/intermediated valent neptunium borates are always isolated.[26,27] When an oxidative-active anion, perchlorate is used in the reaction, *i.e.*, Np(VI) perchlorate is used as a starting material, a Np(VI) borate, $NpO_2[B_8O_{11}(OH)_4]$ can be successfully synthesized.[29]

Single crystal X-ray diffraction study on $NpO_2[B_8O_{11}(OH)_4]$ shows that this compound adopts a noncentrosymmetric framework structure crystallized in the space group *Cc*. A view of the overall structure is shown in Fig. 10a. There is one crystallographically unique neptunyl cation, NpO_2^{2+}, that resides in a hexagonal hole within the polyborate sheets to create a hexagonal bipyramidal environment, AnO_8. Each AnO_8 unit is surrounded by nine borate groups in [*ac*] plane to form an actinyl borate sheet. The sheet topology which is named as the H-Type (Fig. 6) is unique among all actinide borates that we have observed. There are additional BO_3 triangles and BO_4 tetrahedra connecting these actinyl borate sheets together to form the framework structure. It should be noted that this is the only actinyl borate structure type from boric acid reactions where BO_4 tetrahedra are located between the sheets. The twisting of the interlayer borate groups with respect to one another reduces the interlayer space, and yields a less open, denser structure.

The U(VI) and Pu(VI) analogue of $NpO_2[B_8O_{11}(OH)_4]$ can also be made. Thus, the actinide contraction in this series of compounds $AnO_2[B_8O_{11}(OH)_4]$ (An = U, Np, Pu) can be demonstrated with a variety of metrics. First, the unit cell volumes for $UO_2[B_8O_{11}(OH)_4]$, $NpO_2[B_8O_{11}(OH)_4]$, and $PuO_2[B_8O_{11}(OH)_4]$ are 1183.4(5) $Å^3$, 1182.1(2) $Å^3$, and 1180.0(3) $Å^3$, respectively, nicely fit the order of the actinide contraction. More importantly the actinyl An≡O bond distances shrink by 0.02 Å on average from uranium to plutonium. It is important to note that actinyl bonds distances are close enough to each other across the uranium, neptunium, and plutonium series that the actinide contraction is difficult to detect between different types of compounds (*i.e.* the errors in the bond lengths produce overlap if one uses 3σ on the calculated errors). The actinide contraction is only detectable if the errors are small, the residuals are low, and the compounds are isostructural.[72]

The $5f^1$ electron configuration typically yields a single somewhat broad Laporte-forbidden f–f transition in addition to higher energy charge-transfer bands.[73] For U(V) the f–f transition is in the visible region of spectrum.[73] For isoelectronic Np(VI), this transition occurs in the NIR near 1200 nm. The UV-vis-NIR spectra of $NpO_2[B_8O_{11}(OH)_4]$ acquired from a single crystal is shown in Fig. 10b. We have found that this peak can be shifted from where it typically occurs in solution when compared to solid samples. For example, data acquired from single crystals of $NpO_2(NO_3)_2{\cdot}6H_2O$ shows this peak is located at 1100 nm. $NpO_2[B_8O_{11}(OH)_4]$ shows a transition at 1140 nm. In contrast, in single crystals of $NpO_2(IO_3)_2(H_2O)$ the transition is at 1230 nm, which is similar to where it is found in perchlorate and nitrate solutions.[67] Moreover, this transition found in $KNpO_2PO_4{\cdot}3H_2O$ is at 1427 nm. An explanation for the differences in the energy of this transition is the coordination environments of Np(VI). In $NpO_2[B_8O_{11}(OH)_4]$ and $NpO_2(NO_3)_2{\cdot}6H_2O$ the neptunium center is in a hexagonal bipyramidal environment. In $NpO_2(IO_3)_2(H_2O)$ and solutions of neptunyl perchlorate the neptunium is in a pentagonal bipyramidal geometry.[74] In $KNpO_2PO_4{\cdot}3H_2O$, a tetragonal bipyramidal geometry is found for Np(VI).[75] It appears that the addition of a larger number of donor atoms in the equatorial plane, and presumably more electron density at the neptunium center, shifts the f–f transition to higher energy. The reverse effect is observed in the shift of the main transition at 980 nm in Np(V) compounds. Upon the formation of cation–cation interactions, the f–f transition shifts to longer wavelengths.[66]

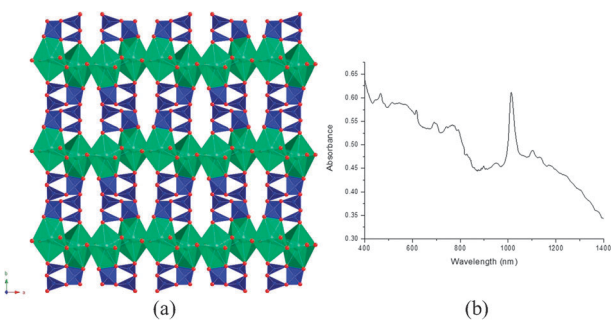

Fig. 9 (a) A depiction of the structure of $NpO_2[B_3O_4(OH)_2]$ showing the sheets of neptunyl cations connected by the polyborate chains. NpO_7 pentagonal bipyramids are shown in green, BO_3 and BO_4 in blue. (b) UV-vis-NIR spectrum of $NpO_2[B_3O_4(OH)_2]$ obtained from a single crystal.

5. Plutonium borates

Plutonium is a highly unusual element, perhaps the most complex in the periodic table, and its chemistry in both aqueous solution and in the solid state are very rich.[76] Five oxidation states including Pu(III), Pu(IV), Pu(V), Pu(VI), and Pu(VII) are accessible in aqueous solution and can be prepared in solid state under the appropriate conditions.[76] The redox chemistry of plutonium is very complicated due to the fact that Pu(III), Pu(IV), Pu(V), Pu(VI) can coexist in solution under a wide range of conditions.[76] Although neptunium in both aqueous solution and solid state is dominated by Np(V) species,[48] several mixed/intermediate valence neptunium borate compounds can still be prepared in boric acid flux as discussed above. It is thus expected that mixed/intermediate-valent plutonium borates can be prepared. However, only monovalent plutonium borates including one Pu(VI) and three Pu(III) borates can be made when plutonium in single oxidation state is used as the starting material.[29,30]

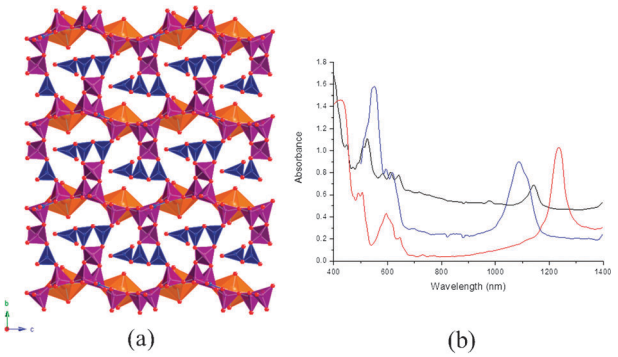

Fig. 10 (a) A depiction of the polar, three-dimensional network found for $NpO_2[B_8O_{11}(OH)_4]$. NpO_8 hexagonal bipyramids are shown in orange, BO_3 triangles in blue, and BO_4 tetrahedra in purple. (b) UV-vis-NIR absorption spectra of the Np(VI) compounds, $NpO_2[B_8O_{11}(OH)_4]$ (black), $NpO_2(NO_3)_2{\cdot}6H_2O$ (blue), and $NpO_2(IO_3)_2(H_2O)$ (red).

5.1 Plutonium(VI) borate

The boric acid flux reaction of Pu(VI) nitrate leads to the formation of the first Pu(VI) borate compound, $PuO_2[B_8O_{11}(OH)_4]$. As mentioned above, this compound is part of the isotypic series $AnO_2[B_8O_{11}(OH)_4]$ (An = U, Np, Pu). $PuO_2[B_8O_{11}(OH)_4]$ can also crystallize in the presence of Ba^{2+} and K^+.[29] However, unlike uranyl and neptunyl borates, additional cations are not readily incorporated into the structure. More importantly, in an effort to make a Pu(IV) borate compound, where Pu(IV) nitrate starting materials was used, the same Pu(VI) borate compound $PuO_2[B_8O_{11}(OH)_4]$ was isolated. The isolation of a Pu(VI) borate from a Pu(IV) source is surprising in light of the fact that Pu(IV) compounds are generally far less soluble and more stable than Pu(VI) compounds.[76]

5.2 Plutonium(III) borates

Unlike trivalent lanthanides, Am(III), or Cm(III), Pu(III) is air-sensitive and is often oxidized to Pu(IV) by oxygen. Although it must be kept in mind that there are some systems (*e.g.* monazites) where Pu(IV) is thermally reduced to Pu(III) at high temperatures.[77] The oxidation of Pu(III) to Pu(IV) can be very rapid at elevated temperatures. When Pu(III) is reacted with molten boric acid at 200 °C or higher it rapidly oxidizes to Pu(IV) and Pu(VI). In order to prevent this oxidation, strictly anaerobic conditions had to be maintained, and it was found that in the absence of oxygen, Pu(III) is maintained in molten boric acid, and we were able to crystallize several Pu(III) borates including $Pu[B_4O_6(OH)_2Cl]$, $Pu_2[B_{13}O_{19}(OH)_5Cl_2(H_2O)_3]$, and $Pu_2[B_{12}O_{18}(OH)_4Br_2(H_2O)_3]{\cdot}0.5H_2O$ using either $PuCl_3$ or $PuBr_3$ as starting Pu(III) sources.[30,32]

Single crystal X-ray diffraction studies show that all three new Pu(III) borates adopt three-dimensional framework structures formed by stacking plutonium(III) polyborate sheets that are very similar to those found with penta- and hexavalent actinides (*e.g.* U(VI), Np(V), Np(VI), and Pu(VI)). These sheets are connected through additional borate units or bridging Cl^- anions. $Pu_2[B_{13}O_{19}(OH)_5Cl_2(H_2O)_3]$ and $Pu_2[B_{12}O_{18}(OH)_4Br_2(H_2O)_3]{\cdot}0.5H_2O$ both contain similar polyborate sheets as shown in Fig. 11b. These sheets contain an unusual unit of three BO_4 tetrahedra that share a common corner (a μ_3-oxo atom). These clusters share corners with BO_3 triangles to create sheets with triangular holes where the Pu(III) cations reside. This sheet topology is named as M-type as shown in Fig. 6 and can also be found in the Ln(III) borate systems, $Ln[B_8O_{11}(OH)_5]$ (Ln = La–Nd) and $Ln[B_9O_{13}(OH)_4]$ (Ln = Pr–Eu).[80] $Pu[B_4O_6(OH)_2Cl]$ possesses a very different sheet topology that lacks the μ_3-oxo atom, and only contains corner-sharing BO_3 and BO_4 units (Fig. 11a). This type of sheet is also known in the Np(V) polyborate sheets in the mixed-valence neptunium borate compound, $K_2[(Np^{VI}O_2)(Np^{V}O_2)_2B_{10}O_{16}(OH)_2(NO_3)_2]$ and described as K-type as shown in Fig. 6. Both types of sheets are joined together by BO_3 or BO_4 units to create three-dimensional networks as shown in Fig. 12.

The most remarkable feature of the three structures of Pu(III) borates is the coordination geometries of Pu(III) centers in these compounds. The coordination geometries of the plutonium centers in these three compounds are shown in Fig. 13. As previously mentioned the plutonium(III) centers reside in triangular holes surrounded by borate units in the polyborate sheets and there are six oxygen donor atoms in these holes that bind the Pu(III) cations. In the structure of $Pu_2[B_{12}O_{18}(OH)_4Br_2(H_2O)_3]{\cdot}0.5H_2O$, there are two crystallographically unique Pu(III) sites. One of these, Pu(1) (Fig. 13a), is nine-coordinate, and the other, Pu(2) (Fig. 13b), is ten-coordinate with the remaining donor atoms above and below the plane of the polyborate sheet.

Both sites are capped on one side by bromide anions. For Pu(1) there is one water molecule and one oxygen atom from bridging BO_3 triangles opposite from the bromide anion, and for Pu(2) there are two water molecules and one oxygen atom from bridging BO_3 triangles. These coordination geometries are not typical for plutonium since the most prevalent coordination environment for nine-coordinate lanthanides and actinides is a tricapped trigonal prism.[78] However, in this compound six of the oxygen atoms are close to being in a plane. The nine-coordinate coordination geometry in $Pu_2[B_{12}O_{18}(OH)_4Br_2(H_2O)_3]{\cdot}0.5H_2O$ is best

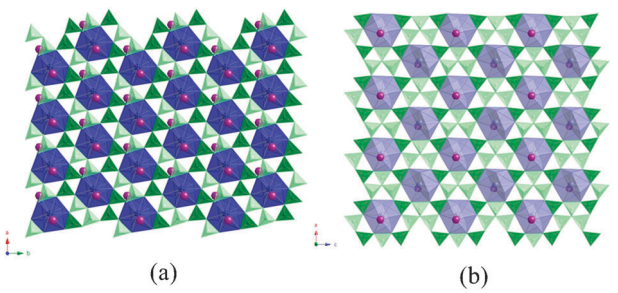

Fig. 11 Views of plutonium polyborate sheets in $Pu[B_4O_6(OH)_2Cl]$ (a), $Pu_2[B_{12}O_{18}(OH)_4Br_2(H_2O)_3]{\cdot}0.5H_2O$ and $Pu_2[B_{13}O_{19}(OH)_5Cl_2(H_2O)_3]$ (b).

described as hula-hoop[78] and the ten-coordinate coordination geometry is capped triangular cupola.[79] Both types of coordination geometries are extremely rare in lanthanide and actinide compounds except for the borate system that are now known.[80–83] All Pu(III) centers in both $Pu[B_4O_6(OH)_2Cl]$ and $Pu_2[B_{13}O_{19}(OH)_5Cl_2(H_2O)_3]$ phases are ten-coordinate and adopt a similar coordination geometry as the Pu2 site in $Pu_2[B_{12}O_{18}(OH)_4Br_2(H_2O)_3]\cdot 0.5H_2O$.[30]

6. Americium borate

Both the aqueous solution and solid-state chemistry of americium is dominated by Am(III), although both Am(III) and Am(VI) are stable in dilute acid conditions while Am(III), Am(IV), Am(V), and Am(VI) are all accessible in alkaline solutions with appropriate complexation.[84] At present, we have successfully synthesized only one Am(III) borate with the formula of $Am[B_9O_{13}(OH)_4]\cdot H_2O$.[32]

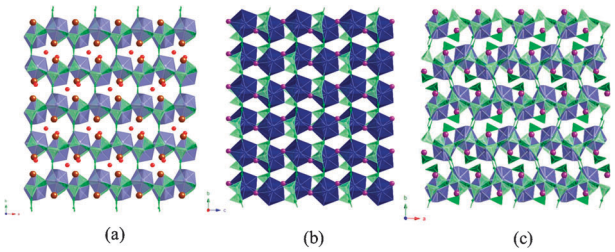

Fig. 12 Depiction of three dimensional framework structures of $Pu_2[B_{12}O_{18}(OH)_4Br_2(H_2O)_3]\cdot 0.5H_2O$ (a), $Pu[B_4O_6(OH)_2Cl]$ (b), and $Pu_2[B_{13}O_{19}(OH)_5Cl_2(H_2O)_3]$ (c).

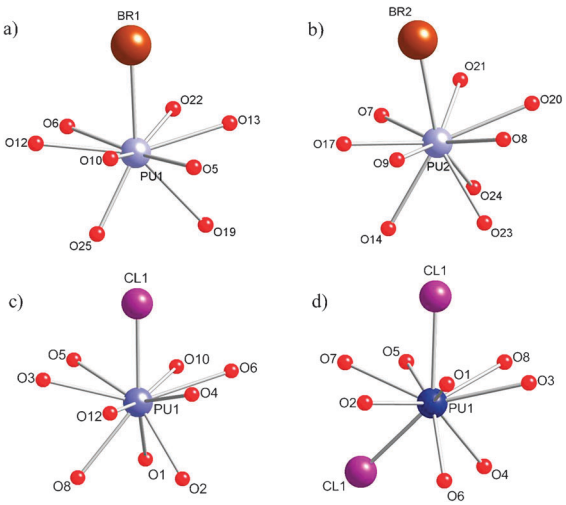

Fig. 13 Views of coordination environments of all plutonium sites in $Pu_2[B_{12}O_{18}(OH)_4Br_2(H_2O)_3]\cdot 0.5H_2O$ (a and b), $Pu[B_4O_6(OH)_2Cl]$ (d), and $Pu_2[B_{13}O_{19}(OH)_5Cl_2(H_2O)_3]$ (c).

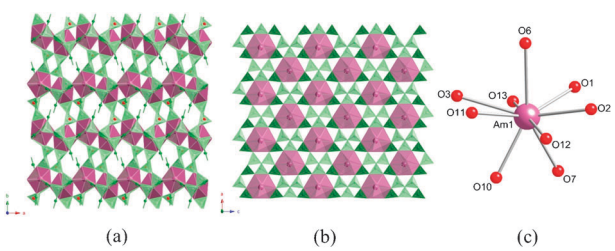

Fig. 14 (a) Depiction of the three-dimensional framework structure of $Am[B_9O_{13}(OH)_4]\cdot H_2O$. (b) A view of americium polyborate sheets in $Am[B_9O_{13}(OH)_4]\cdot H_2O$. (c) Coordination environments of americium sites in $Am[B_9O_{13}(OH)_4]\cdot H_2O$.

$Am[B_9O_{13}(OH)_4]\cdot H_2O$ was made *via* boric acid flux reaction using $AmCl_3$ as the starting material at 240 °C. The crystal structure of $Am[B_9O_{13}(OH)_4]\cdot H_2O$ is similar with two of the Pu(III) borates, $Pu_2[B_{13}O_{19}(OH)_5Cl_2(H_2O)_3]$ and $Pu_2[B_{12}O_{18}(OH)_4Br_2(H_2O)_3]\cdot 0.5H_2O$. As observed in these two Pu(III) borates, $Am[B_9O_{13}(OH)_4]\cdot H_2O$ also adopted a dense, three-dimensional structure shown in Fig. 14a. The structure of $Am[B_9O_{13}(OH)_4]\cdot H_2O$ is formed based on the polyborate sheet type that is identical with $Pu_2[B_{13}O_{19}(OH)_5Cl_2(H_2O)_3]$ and $Pu_2[B_{12}O_{18}(OH)_4Br_2(H_2O)_3]\cdot 0.5H_2O$ (Fig. 14b). However, obvious differences can also be observed between the Am(III) and Pu(III) borates. As given by the formula, $Am[B_9O_{13}(OH)_4]\cdot H_2O$ lacks halide entirely, and this is a significant departure from the reactivity of Pu(III) halide starting materials where we observe halides bound to Pu(III) in the final products. Moreover, the Am(III) in $Am[B_9O_{13}(OH)_4]\cdot H_2O$ is solely nine-coordinate while ten-coordinate geometry (Fig. 14c) dominates the three Pu(III) borates. The capping group for $Am[B_9O_{13}(OH)_4]\cdot H_2O$ where the halide would have been is instead occupied by a BO_3 unit that bridges to the next layer. The two sites beneath the borate layer are two oxo atoms in one BO_4 unit.

The differences observed between the Am(III) borate and Pu(III) borates is rather striking, and can be ascribed to several changes between these two elements. First, the actinide contraction between Pu(III) and Am(III) is larger than one might expect. Pu(III) has an ionic radius of 1.00 Å; whereas Am(III) has a radius of 0.975 Å (CN = 6).[85] Typical changes between the ionic radius of neighbouring rare earth elements is usually closer to 0.01 Å. Therefore, the formation of a different structure is not completely surprising. Second, while exclusion of chloride from the inner coordination sphere is a bit more perplexing, it is also a reflection of the increased Pearson hardness of the Am(III) cation *versus* the Pu(III) cation. Am(III) clearly prefers all oxo donors. Finally, $Pu_2[B_{13}O_{19}(OH)_5Cl_2(H_2O)_3]$ does not have a lanthanide analog whereas lanthanides with similar structures to $Am[B_9O_{13}(OH)_4]\cdot H_2O$ are known.[80–83] Thus this represents a sharp demarcation between the chemistry of Pu(III) and Am(III) where

involvement of the 5f orbitals in bonding is largely lost with Am(III), and there is a larger contraction in ionic radius than one might anticipate.

Conclusions

We have prepared a large family of exotic actinide borates using molten boric acid flux reactions. The solid-state chemistry and physical properties of these compounds is unprecedented. We have provided evidence that the behavior of actinide elements in molten boric acid is substantially different from that observed in aqueous solutions. The unprecedented chemistry of these compounds is represented by the extremely rare cationic framework thorium borate that can selectively remove TcO_4^- from nuclear waste streams, extraordinarily complicated mixed/intermediate-valent neptunium borates that can simultaneously contain neptunium in three different oxidation states, new coordination environments for An(III), and the divergent behavior of Pu(III) and Am(III). Actinide borates show remarkable structural diversity that has never been observed in any other ligand systems in solid-state actinide chemistry. Borate is a non-redox-active ligand that can be used to structurally probe small differences among different elements, oxidation states, or even reaction conditions while providing a variety of donor atoms to metal centers with different geometric preferences.

One important lesson to be taken from this work is that great caution needs to be exercised in predicting the chemistry of transuranium materials based on the behaviour of uranium compounds; they can be exceedingly different. Even neighbouring elements in the same oxidation states can show obviously different structures and coordinate geometries.

Acknowledgements

We are grateful for support provided by the Chemical Sciences, Geosciences, and Biosciences Division, Office of Basic Energy Sciences, Office of Science, Heavy Elements Program, U.S. Department of Energy, under Grant DE-FG02-01ER16026, DE-SC0002215 and by Deutsche Forschungsgemeinschaft for support within the DE 412/43-1 research project. This material is based upon work supported as part of the Materials Science of Actinides, an Energy Frontier Research Center funded by the U.S. Department of Energy, Office of Science, Office of Basic Energy Sciences under Award Number DE-SC0001089.

Notes and references

1 T. Nakano and E. Nakamura, *Phys. Earth Planet. Inter.*, 2001, **127**, 233–252.
2 S. R. Taylor, *Geochim. Cosmochim. Acta*, 1964, **28**, 1273–1285.
3 P. C. Burns, R. C. Ewing and F. C. Hawthorne, *Can. Mineral.*, 1997, **35**, 1551–1570.
4 P. C. Burns, *Can. Mineral.*, 2005, **43**, 1839–1894.
5 P. C. Burns, M. L. Miller and R. C. Ewing, *Can. Mineral.*, 1996, **34**, 845–880.
6 (*a*) I. A. Donald, B. L. Metcalfe and R. N. J. Taylor, *J. Mater. Sci.*, 1997, **32**, 5851–5887; (*b*) W. E. Lee, M. I. Ojovan, M. C. Stennett and N. C. Hyatt, *Adv. Appl. Ceram.*, 2006, **105**, 3–12.
7 B. Grambow, *Elements*, 2006, **2**, 357–364.
8 W. Lutze, *Glass*, in *Uncertainty Underground*, ed. A. M. Macfarlane and R. C. Ewing, The MIT Press, London, 2006, ch. 21, pp. 353–364.
9 A. C. Snider, Verification of the Definition of Generic Weep Brine and the Development of a Recipe for This Brine. ERMS 527505. Carlsbad, NM: Sandia National Laboratories, 2003.
10 M. Borkowski, M. Richmann, D. T. Reed and Y. Xiong, *Radiochim. Acta*, 2010, **98**, 577–582.
11 H. Behm, *Acta Crystallogr., Sect. C: Cryst. Struct. Commun.*, 1985, **41**, 642–645.
12 M. Gasperin, *Acta Crystallogr., Sect. C: Cryst. Struct. Commun.*, 1987, **43**, 1247–1250.
13 M. Gasperin, *Acta Crystallogr., Sect. C: Cryst. Struct. Commun.*, 1987, **43**, 2031–2033.
14 M. Gasperin, *Acta Crystallogr., Sect. C: Cryst. Struct. Commun.*, 1987, **43**, 2264–2266.
15 M. Gasperin, *Acta Crystallogr., Sect. C: Cryst. Struct. Commun.*, 1988, **44**, 415–416.
16 M. Gasperin, *Acta Crystallogr., Sect. C: Cryst. Struct. Commun.*, 1989, **45**, 981–983.
17 M. Gasperin, *Acta Crystallogr., Sect. C: Cryst. Struct. Commun.*, 1990, **46**, 372–374.
18 A. Cousson and M. Gasperin, *Acta Crystallogr., Sect. C: Cryst. Struct. Commun.*, 1991, **47**, 10–12.
19 D. L. Clark, D. E. Hobart and M. P. Neu, *Chem. Rev.*, 1995, **95**, 25–48.
20 S. Wang, E. V. Alekseev, J. Diwu, W. H. Casey, B. L. Phillips, W. Depmeier and T. E. Albrecht-Schmitt, *Angew. Chem., Int. Ed.*, 2010, **49**, 1057–1060.
21 P. Yu, S. Wang, E. V. Alekseev, W. Depmeier, T. E. Albrecht-Schmitt, B. Phillips and W. Casey, *Angew. Chem. Int. Ed.*, 2010, **49**, 5975–5977.
22 S. Wang, E. V. Alekseev, J. Ling, G. Liu, W. Depmeier and T. E. Albrecht-Schmitt, *Chem. Mater.*, 2010, **22**, 2155–2163.
23 S. Wang, E. V. Alekseev, J. T. Stritzinger, W. Depmeier and T. E. Albrecht-Schmitt, *Inorg. Chem.*, 2010, **49**, 2948–2953.
24 S. Wang, E. V. Alekseev, J. T. Stritzinger, W. Depmeier and T. E. Albrecht-Schmitt, *Inorg. Chem.*, 2010, **49**, 6690–6696.
25 S. Wang, E. V. Alekseev, J. T. Stritzinger, G. Liu, W. Depmeier and T. E. Albrecht-Schmitt, *Chem. Mater.*, 2010, **22**, 5983–5991.
26 S. Wang, E. V. Alekseev, J. Ling, S. Skanthakumar, L. Soderholm, W. Depmeier and T. E. Albrecht-Schmitt, *Angew. Chem., Int. Ed.*, 2010, **49**, 1263–1266.
27 S. Wang, E. V. Alekseev, W. Depmeier and T. E. Albrecht-Schmitt, *Chem. Commun.*, 2010, **46**, 3955–3957.
28 S. Wang, E. V. Alekseev, H. M. Miller, W. Depmeier and T. E. Albrecht-Schmitt, *Inorg. Chem.*, 2010, **49**, 9755–9757.
29 S. Wang, E. M. Villa, J. Diwu, E. V. Alekseev, W. Depmeier and T. E. Albrecht-Schmitt, *Inorg. Chem.*, 2011, **50**, 2527–2533.
30 S. Wang, E. V. Alekseev, W. Depmeier and T. E. Albrecht-Schmitt, *Inorg. Chem.*, 2011, **50**, 2079–2081.
31 S. Wang, E. V. Alekseev, J. Diwu, H. M. Miller, A. Oliver, G. Liu, W. Depmeier and T. E. Albrecht-Schmitt, *Chem. Mater.*, 2011, **23**, 2931–2939.
32 M. J. Polinski, S. Wang, E. V. Alekseev, W. Depmeier and T. E. Albrecht-Schmitt, *Angew. Chem., Int. Ed.*, 2011, **50**, 8891–8894.
33 A. Callegari, F. Caucia, F. Mazzi, R. Oberti, L. Ottolini and L. Ungaretti, *Am. Mineral.*, 2000, **85**, 586–593.
34 M. Boiocchi, A. Callegari, L. Ottolini and A. Maras, *Am. Mineral.*, 2004, **89**, 1540–1545.
35 M. Boiocchi, A. Callegari and L. Ottolini, *Am. Mineral.*, 2006, **91**, 1170–1177.
36 R. Oberti, L. Ottolini, F. Camara and G. della Ventura, *Am. Mineral.*, 1999, **84**, 913–921.
37 G. della Ventura, P. Bonazzi, R. Oberti and L. Ottolini, *Am. Mineral.*, 2002, **87**, 739–744.
38 S. P. Mushran, *Nature*, 1946, **158**, 95.
39 V. Rives, *LDHs: Layered Double Hydroxides: Present and Future*, Nova Science Publishers Inc., Hauppauge, New York, USA, 2001.
40 D. G. Evans and R. C. T. Slade, *Layered Double Hydroxides*, Springer-Verlag, New York, NY, USA, 2006.
41 S. R. Oliver, *Chem. Soc. Rev.*, 2009, **38**, 1868–1881.
42 H. V. Goulding, S. E. Hulse, W. Clegg, R. W. Harrington, H. Y. Playford, R. I. Walton and A. M. Fogg, *J. Am. Chem. Soc.*, 2010, **132**, 13618–13620.
43 H. Fei, D. L. Rogow and S. R. J. Oliver, *J. Am. Chem. Soc.*, 2010, **132**, 7202–7209.
44 E. V. Alekseev, S. V. Krivovichev and W. Depmeier, *Angew. Chem., Int. Ed.*, 2008, **47**, 549–551.
45 K. M. Ok, J. Sung, G. Hu, R. M. J. Jacobs and D. O'Hare, *J. Am. Chem. Soc.*, 2008, **130**, 3762–3763.
46 R. E. Wilson, S. Skanthakumar, K. E. Knope, C. L. Cahill and L. Soderholm, *Inorg. Chem.*, 2008, **47**, 9321–9326.
47 J. P. Kaszuba and W. H. Runde, *Environ. Sci. Technol.*, 1999, **33**, 4427–4433.
48 Z. Yoshida, S. G. Johnson, T. Kimura and J. R. Krsul, *Neptunium*, in *The Chemistry of the Actinide and Transactinide Elements*, ed. L. R. Morss, N. M. Edelstein and

J. Fuger, Springer, The Netherlands, 2006, vol. 2, ch. 6, pp. 753–770.
49 T. H. Bray, J. Ling, E. S. Choi, J. S. Brooks, J. V. Beitz, R. E. Sykora, R. G. Haire, D. M. Stanbury and T. E. Albrecht-Schmitt, *Inorg. Chem.*, 2007, **46**, 3663–3668.
50 L. Rao, *Chem. Soc. Rev.*, 2007, **36**, 881–892.
51 M. Buhl, G. Schreckenbach, N. Sieffert and G. Wipff, *Inorg. Chem.*, 2009, **48**, 9977–9979.
52 A. K. Pikaev, A. V. Gogolev and V. P. Shilov, *Radiat. Phys. Chem.*, 1999, **56**, 483–491.
53 P. Almond, R. Sykora, S. Skanthakumar, L. Soderholm and T. Albrecht-Schmitt, *Inorg. Chem.*, 2004, **43**, 958–963.
54 I. Charushnikova, E. Boss, D. Guillaumont and P. Moisy, *Inorg. Chem.*, 2010, **49**, 2077–2082.
55 S. Cornet, L. Häller, M. Sarsfield, D. Collison, M. Helliwell, I. May and N. Kaltsoyannis, *Chem. Commun.*, 2009, 917–919.
56 M. Grigor'ev, A. Fedoseev and N. Budantseva, *Russ. J. Coord. Chem.*, 2003, **29**, 877–879.
57 P. C. Burns, K.-A. Kubatko, G. Sigmon, B. J. Fryer, J. E. Gagnon, M. R. Antonio and L. Soderholm, *Angew. Chem., Int. Ed.*, 2005, **44**, 2135–2139.
58 P. C. Burns, J. D. Grice and F. C. Hawthorne, *Can. Mineral.*, 1995, **33**, 1131–1151.
59 J. D. Grice, P. C. Burns and F. C. Hawthorne, *Can. Mineral.*, 1999, **37**, 731–762.
60 G. Yuan and D. Xue, *Acta. Cryst.*, 2007, **B63**, 353–362.
61 E. L. Belokoneva, *Cryst. Res. Technol.*, 2008, **43**, 1173–1182.
62 M. Touboul, N. Penin and G. Nowogrocki, *Solid State Sci.*, 2003, **5**, 1327–1342.
63 C. Dendrinou-Samara, C. M. Zaleski, A. Evagorou, J. W. Kampf, V. L. Pecoraro and D. P. Kessissoglou, *Chem. Commun.*, 2003, 2668–2669.
64 T. Okubo, H. Kuwamoto, K. H. Kim, S. Hayami, A. Yamano, M. Shiro, M. Maekawa and T. Kuroda-Sowa, *Inorg. Chem.*, 2011, **50**, 2708–2710.
65 J. C. Sullivan, J. C. Hindman and A. J. Zielen, *J. Am. Chem. Soc.*, 1961, **83**, 3373–3378.
66 N. N. Krot and M. S. Grigor'ev, *Russ. Chem. Rev.*, 2004, **73**, 89–100.
67 H. A. Friedman and L. M. Toth, *J. Inorg. Nucl. Chem.*, 1980, **42**, 1347–1349.
68 N. M. Edelstein, *Magnetic Properties*, in *The Chemistry of the Actinide and Transactinide Elements*, ed. L. R. Morss, N. M. Edelstein and J. Fuger, Springer, The Netherlands, 2006, vol. 4, ch. 20, pp. 2225–2306.
69 T. Nakamoto, M. Nakada and A. Nakamura, *Solid State Commun.*, 2001, **119**, 523–526.
70 T. Z. Forbes, P. C. Burns, S. Skanthakumar and L. Soderholm, *J. Am. Chem. Soc.*, 2007, **129**, 2760–2761.
71 T. Z. Forbes, C. Wallace and P. C. Burns, *Can. Mineral.*, 2008, **46**, 1623–1645.
72 C. Apostolidis, B. Schimmelpfennig, N. Magnani, P. Lindqvist-Reis, O. Walter, R. Sykora, A. Morgenstern, E. Colineau, R. Caciuffo, R. Klenze, R. G. Haire, J. Rebizant, F. Bruchertseifer and T. Fanghanel, *Angew. Chem., Int. Ed.*, 2010, **49**, 6343–6347.
73 G. Liu and J. V. Beitz, *Spectra and Electronic Structures of Free Actinide Atoms*, in *The Chemistry of the Actinide and Transactinide Elements*, ed. L. R. Morss, N. M. Edelstein and J. Fuger, Springer, The Netherlands, 2006, vol. 4, ch. 16, pp. 2013–2111.
74 A. C. Bean, B. L. Scott, T. E. Albrecht-Schmitt and W. Runde, *Inorg. Chem.*, 2003, **42**, 5632–5636.
75 T. Z. Forbes and P. C. Burns, *Can. Mineral.*, 2007, **45**, 471–477.
76 D. L. Clark, S. S. Hecker, G. D. Jarvinen and M. P. Neu, *Plutonium*, in *The Chemistry of the Actinide and Transactinide Elements*, ed. L. R. Morss, N. M. Edelstein and J. Fuger, Springer, The Netherlands, 2006, vol. 2, ch. 7, pp. 813–1264.
77 C. E. Bambergera, R. G. Haire, H. E. Hellwege and G. M. Begun, *J. Less Common Met.*, 1984, **97**, 349–356.
78 A. Ruiz-Martínez, D. Casanova and S. Alvarez, *Chem.–Eur. J.*, 2008, **14**, 1291–1303.
79 A. Ruiz-Martínez and S. Alvarez, *Chem.–Eur. J.*, 2009, **15**, 7470–7480.
80 L. Li, X. Jin, G. Li, Y. Wang, F. Liao, G. Yao and J. Lin, *Chem. Mater.*, 2003, **15**, 2253–2260.
81 P. Lu, Y. Wang, J. Lin and L. You, *Chem. Commun.*, 2001, 1178–1179.
82 L. Li, P. Lu, Y. Wang, X. Jin, G. Li, Y. Wang, L. You and J. Lin, *Chem. Mater.*, 2002, **14**, 4963–4968.
83 E. L. Belokoneva, S. Yu. Stefanovich, O. V. Dimitrova and A. G. Ivanova, *Zhurnal Neorganicheskoi Khimii*, 2002, **47**, 370–377.
84 W. H. Runde and W. W. Schulz, *Americium*, in *The Chemistry of the Actinide and Transactinide Elements*, ed. L. R. Morss, N. M. Edelstein and J. Fuger, Springer, The Netherlands, 2006, vol. 2, ch. 8, pp. 1265–1395.
85 R. D. Shannon, *Acta Crystallogr., Sect. A: Cryst. Phys., Diffr., Theor. Gen. Crystallogr.*, 1976, **32**, 751–767.